Received: 23 March 2021 | Revised: 10 January 2022 | Accepted: 28 January 2022

DOI: 10.33012/navi.513

ORIGINAL ARTICLE

Positioning and Velocity Performance Levels for a Lunar Lander using a Dedicated Lunar Communication and Navigation System

Antoine Grenier[1] | **Pietro Giordano**[1] | **Lorenzo Bucci**[2] | **Alexander Cropp**[1] | **Paolo Zoccarato**[1] | **Richard Swinden**[1] | **Javier Ventura-Traveset**[3]

[1] European Space Research and Technology Centre (ESTEC), European Space Agency

[2] European Space Operations Centre (ESOC), European Space Agency

[3] Centre Spatial de Toulouse, European Space Agency

Correspondence
Pietro Giordano
European Space Research and Technology Centre (ESTEC), European Space Agency
Noordwijk, Netherlands
Email: pietro.giordano@esa.int
+31 (0)71 56 53003

Abstract

The interest in Moon exploration has grown substantially in the last few years, appointing the Moon as the first step toward deep space exploration. However, the current state-of-the-art approach for lunar landing does not always reach the required performance levels. This contribution presents a potential implementation of a dedicated lunar communication and navigation service (LCNS) and the performance levels achievable by a representative lunar lander mission that uses the LCNS. The expected positioning precision during the final descent and at the landing site is demonstrated here with a variance-covariance analysis starting from reasonable assumptions about the capabilities of a potential dedicated LCNS system. The performance in positioning and navigation achievable during a generic moon-landing phase significantly outperforms existing ground-based baseline solutions, enabling the stringent requirements from the International Space Exploration Coordination Group (ISECG) to be met.

1 | INTRODUCTION

With the Moon becoming the next long-term objective in space for both agencies (ESA, 2021; NASA, 2021) and private actors (NASA, 2020), the number of expected missions to Earth's natural satellite might exceed, already in this decade, the overall number reached in the 1960s–1970s (Euroconsult, 2020).

In the past, lunar missions have almost entirely relied on direct-to-Earth (DTE) communications, whilst using ranging radiometric measurements from Earth for navigation. The benefits of a lunar relay infrastructure were already envisaged in the early years of the Apollo missions (Farquhar, 1971) and were also demonstrated by the recent far-side landing of the Chinese Chang'E 4 mission (Gao et al., 2019; the latter focused on relaying telemetry to ground rather than providing an independent orbit determination and navigation solution). The growing trend in the number of missions to the Moon is creating demand for the deployment of a lunar communication and navigation infrastructure to support the international community. This, in turn, can act as a catalyst for additional public and private worldwide cislunar initiatives.

In terms of navigation services, studies have already shown that GNSS signals from Earth can be received at the Moon's altitude (Capuano et al., 2016; Delépaut et al., 2020; Winternitz et al., 2019), effectively providing support for orbit determination and landing operations on the near-side. However, this technology alone does not support far-side operations and will not reach the accuracy required by the *Global Exploration Roadmap Critical Technology Needs* (ISECG, 2019).

Landing on the Moon has been successfully performed since the initial phase of lunar exploration, both with human and robotic missions; however, recent failures (e.g., Halon [2019] and Guptan [2019]) have shown that landing on Earth's natural satellite is actually not an easy task. Furthermore, to land with a 90-meter 3-sigma uncertainty from the target landing location, as required by the *Global Exploration Roadmap Critical Technology Needs* (ISECG, 2019), is considered very challenging. However, there have been demonstrations of landing accuracies down to 40 meters terrestrially using NASA's Jet Propulsion Laboratory lander vision system (Johnson et al., 2017), and the recent landing on Mars (NASA Mars 2020 Mission) has also now demonstrated this system's level of reliability. It may be feasible to reuse this technology for lunar landing, even if a detailed assessment of the specific features and image quality of the lunar landing areas would still need to be performed.

In recent years, several space agencies have proposed dedicated systems to address these problems and provide navigation and communication services to future lunar missions. In particular, the Russian satellite maker, Information Satellite Systems (ISS) JSC, proposed a full constellation of 24 satellites around the Moon (Russians News Agency, 2020), while NASA has proposed LunaNET (Israel et al., 2020).

The topic has been widely discussed in the literature since the 1970s when Farquhar described how satellites in Earth-Moon libration points could be used to support satellite navigation in cislunar space (Farquhar, 1971). This work has been further extended in Carpenter et al. (2004), in which the author assessed different lunar navigation infrastructures based on Earth-Moon Lagrange point orbiters providing one-way Doppler measurements together with Earth GPS signals showing results better than 1 km for positioning and 5 cm/s for velocity in cislunar space.

In more recent years, NASA introduced the Cislunar Autonomous Positioning System (CAPS; Parker et al., 2019) that aims to provide autonomous navigation in cislunar space for satellites (or nodes in general) that participate in the CAPS network. The concept is based on the LiASON (Linked Autonomous Interplanetary Satellite Orbit Navigation) concept and uses inter-satellite link range and range-rate measurements between cooperating satellites together with knowledge of the characteristics of the gravity field influencing both satellites to compute relative and inertial absolute positioning. The concept has shown to provide very good autonomous results and is planned to be demonstrated in space with the CAPSTONE missions, currently scheduled for launch in 2022 (Cheetham, 2020).

In this context, the European Space Agency (ESA) has proposed a concept called *Moonlight* that aims to provide communication and navigation services to institutional and commercial lunar missions (ESA, 2020). The ESA's vision represented by the Moonlight initiative is to foster the creation and development of dedicated lunar communication and navigation services. These services will support the next generation of institutional and private lunar exploration missions, including enhancing the performance of those missions currently under definition and creating new possibilities. A high-level view of some potential navigation aspects of Moonlight has been presented in Schönfeldt et al. (2020a, 2020b). The navigation service foreseen for Moonlight is similar to other concepts already presented in

the literature (Barton et al., 1993; Chen et al., 2017; Circi et al., 2014; MacNicol & Raquet, 2002) that aim to provide one-way broadcast radio navigation signals that allow a user to compute its position and velocity and to synchronize its local clock to a reference time.

Overall, the goals and concept of the Moonlight navigation service are closely aligned with the ones defined by Barton et al. (1993), except that Moonlight takes advantage of GNSS satellite technology evolutions (for satellite, ground, and user) to make a one-way broadcast solution a viable option. This allows them to maintain the possibility of implementing an additional two-way navigation service as proposed in Barton et al. (1993) and further discussed in Schönfeldt et al. (2020a, 2020b).

The extensive and intentional reuse of GNSS technology, both at the system and user level, is a pillar of the Moonlight navigation service. One last critical aspect not addressed in other publications is the requirement to keep the user terminal and mission operational concept as simple and cost effective as possible. While other concepts propose the use of two-way ranging or Doppler-based measurements, Moonlight aims to reuse the modulations, navigation techniques, satellite payload, and user terminal technologies from GNSS.

This contribution presents the potential implementation of a dedicated *lunar communication and navigation service* (LCNS), provides assumptions made at the system level from orbit to signal transmission, and presents how potential lunar missions can exploit the LCNS navigation service. Levels of performance are assessed using a variance-covariance analysis and, as such, the results presented in this publication provide order of magnitude levels of expected performance.

The analysis addresses a potential lunar lander mission, focusing on the final descent from lunar orbit to touchdown. Section 2 describes the mission profile considered in this analysis. Section 3 presents the different assumptions of the LCNS system design, adopted measurements, and system/user concept of operations. A user device receiving the LCNS signal is also described in Section 4, providing details about the user navigation filter. Section 5 reports the results of the variance analysis, presenting the expected positioning precision during the final descent and touchdown. Finally, Section 6 addresses the conclusions and future work.

2 | LANDER MISSION PROFILE

The mission profile considered in this contribution is a lunar lander, targeting a landing site close to the lunar south pole. The main mission phases are described in the following section, focusing on the spacecraft's arrival in lunar orbit, the low lunar orbit (LLO) phase, and the final descent—these are the phases in which the presence of a lunar navigation infrastructure would be the most beneficial. This section also illustrates the approach based on the current state-of-the-art technology and techniques (i.e., without using a dedicated lunar radio navigation system).

2.1 | Lunar Transfer Orbit (LTO)

The transfer to the Moon generally employs a *lunar transfer orbit* (LTO) with an apogee of 400,000 km, obtained by direct injection from the launch vehicle or after a *geosynchronous/geostationary transfer orbit* (GTO) launch and a perigee burn. During this phase, navigation is typically performed with ground stations and radiometric measurements (range and Doppler).

No significant benefit was identified when using the LCNS for the LTO, except for redundancy and a possible reduction of operational costs[1]. At least two trajectory correction maneuvers (TCMs) are scheduled during this phase to correct the launcher injection error and target the proper orbital injection upon arrival at the Moon. This phase is not assessed in the variance-covariance analysis of this contribution.

2.2 | Low Lunar Orbit (LLO)

After arriving at the Moon, the spacecraft is injected into a circular *low lunar orbit* (LLO) by a maneuver of about 850 m/s. Here, a loitering phase is required to align the orbital plane with the landing site and ensure proper illumination conditions will be available during landing. Currently, the minimum duration of such a loitering phase is driven by the *orbit determination* (OD) requirements, since at least four days are envisaged (two days tracking and two days ground processing) prior to descent initiation.

This requirement has a significant impact on the mission design, and the reduction of the minimum time for OD would enable a more flexible LLO phase, with relaxed constraints on its minimum duration. The accuracy of ground-based measurements depends on several factors: spacecraft transponder noise level, ground stations availability, measurements type, etc. (Miller, 2019). A comprehensive analysis of this accuracy is outside the scope of this paper.

2.3 | Descent

The descent phase lasts about one hour and is initiated by the periselene lowering burn, followed by a coasting phase in an elliptical LLO. After this phase, the main braking burn is commanded and the spacecraft performs a powered descent to reduce the orbital velocity until reaching the high gate altitude (HGA) around 2 km above the lunar surface. The spacecraft will continue to reduce the horizontal velocity and pitch down until the thrusters point toward the surface.

When the spacecraft reaches a point 20 m directly above the desired landing location, it will descend vertically at a fixed velocity until touchdown. This profile is based on the future *European Large Logistics Lander* (EL3) mission, part of the ESA roadmap to the Moon (ESA, 2021). Currently, EL3 plans to use the pilot module containing a range of sensors to support navigation to the Moon's surface. Details on this can be found in *Spacewatch Europe* (2021).

The current state-of-the-art technology allows for landing within a few hundreds of meters from the target location (e.g., within an ellipse with axes of approximately 500 x 300 meters). Even if this level of performance is already outstanding, it is not sufficient to cover the specific needs identified in the *Global Exploration Roadmap Critical Technology Needs*, which requires 90-m 3-sigma landing accuracy from the target landing location (ISECG, 2019; e.g., GER-018—precision landing with hazard avoidance).

The landing site selected for this study is located close to the Schrödinger crater (-75.00000°N, 140.99318°E), a site identified by the scientific community for future exploration and being considered by the ESA for future lunar landing missions

[1] For this phase, instead, the use of Earth GNSS constellations with high-sensitive receivers for navigation could prove to be highly beneficial as explained in Schönfeldt et al. (2020).

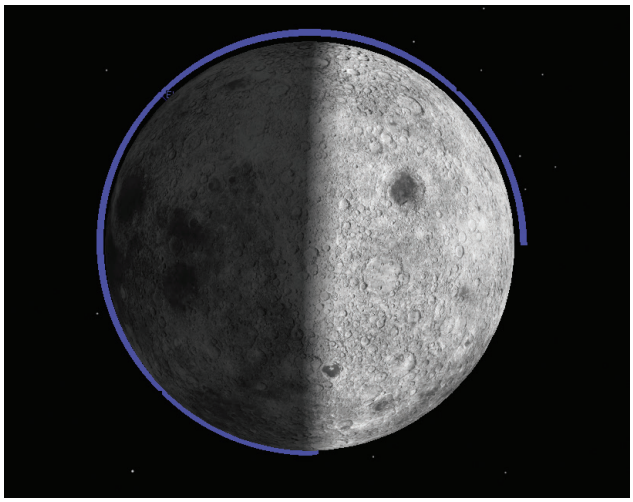

FIGURE 1 LLO and final descent

(ESA, 2019). This landing location is on the Moon's far side, which increases the mission complexity due to a lack of DTE link during the final descent.

3 | MOONLIGHT AND LCNS

The Moonlight initiative (ESA, 2020) and the LCNS are still under definition, therefore it is not currently possible to assess their performance levels specifically. In this contribution, for the sake of illustration and in order to perform a concrete analysis, one possible option for a lunar satellite constellation is considered which is based on the ESA's internal studies. Even if the final constellation for the LCNS is different, the analysis and results presented in this paper can easily be extended to other lunar constellation options.

The LCNS is expected to provide different navigation services, among which there is a one-way service similar to the one provided by Earth GNSS systems. The concept behind this service is the same as for Earth GNSS: the user position, velocity, and time can be computed based on a standard time-of-arrival approach, assuming that all the signals received by multiple satellites are synchronized. Estimated synchronization errors and satellite orbits are provided in a dedicated navigation message broadcasted within the signal. Such a service presents many advantages, the most important being the high level of technology reuse, both at the system and user level, reducing the time to market significantly and easing the introduction of the user equipment in future space missions. It is also expected that the user receivers could be a simple evolution of spaceborne GNSS receivers, which are already widely used today.

This approach should facilitate the use of Moonlight navigation receivers in lunar missions by reducing the complexity of the user terminal integration with the hosting satellite/lander/rover and easing the mission's operational concept. This is thanks to the extensive heritage from GNSS on Earth and due to the possibility of using a single user terminal for all types of missions (with potentially only software modifications needed to adapt to the specific mission dynamics).

The concept has several advantages over different concepts such as CAPS, (Parker et al., 2019) and two-way navigation (Barton et al., 1993):

- The user mission does not need to actively transmit via inter-satellite link, leading to a reduced terminal size, weight, and power (SWaP).
- The user navigation terminal SWaP is very small and a simple evolution of the currently available spaceborne GNSS receivers.
- The service will ensure high levels of accuracy in all conditions, with fast state vector computation for surface rovers that might not achieve such high levels of performance based on collaborative inertial concepts.

The use of radio frequency navigation signals provided by a dedicated lunar system aims to provide a redundant sensor and, eventually, an alternative to the fully autonomous visual-based landing techniques (Johnson et al., 2017) allowing for the reduction of the mass, weight, and power of the landing navigation unit. In fact, the use of an LCNS would remove the need for visual cameras and digital components required to process the images onboard and, more importantly, remove auxiliary sensors such as radar Doppler altimeters that are normally heavy (around 10 kg including antennas). An LCNS receiver is expected to be very similar to a spaceborne GNSS receiver with a mass around 2–3 kg, including antennas.

As such, the use of LCNS rather than visual-based navigation can lead to significant cost saving when considering a price of €500,000 to €1,000,000 per kilogram of payload to be taken to the Moon. In addition, the same LCNS receiver used during landing can be used for ground operations, making it a multi-purpose unit, while normally not all the visual-based sensors used during landing are reused during the ground mission. Finally, an LCNS will also allow missions to land close to or within permanently shadowed areas that are of great interest to the scientific community, without risk of mission loss due to a lack of visual landmarks.

Details on Moonlight and LCNS can be found in Schönfeldt et al. (2020a, 2020b) and ESA (2020).

3.1 | Lunar Communication and Navigation Service

The LCNS constellation considered in this publication is based on satellites orbiting the Moon in *elliptical lunar frozen orbits* (ELFOs). These orbits were selected for their coverage of the Moon's south pole, which is the region of interest for several planned missions, as well as for their stability over time, minimizing the need for orbit-keeping maneuvers. This constellation is composed of five satellites, located in three different ELFO planes, wherein each plane is separated by 120°. The orbital parameters of these five satellites can be found in Table 1.

The true anomalies of the orbits were computed in order to optimize the overall GDOP figure on the Moon's surface. The first three satellites (1-2-3) are designed to have an equal time-based separation along their orbits (i.e., with a uniform spacing

TABLE 1
ELFO Keplerian Parameters of LCNS Satellites

Satellite number	SMA	Ecc.	Inclination	Arg. Per.	RAAN	TA
1	9,750.7 km	0.7	63.2°	90°	0°	0°
2	9,750.7 km	0.7	63.2°	90°	120°	164°
3	9,750.7 km	0.7	63.2°	90°	240°	196°
4	9,750.7 km	0.7	63.2°	90°	120°	245°
5	9,750.7 km	0.7	63.2°	90°	240°	184°

TABLE 2
LCNS Navigation Payload Characteristics

Parameters	Values
EIRP at boresight	11.5 dBW
Modulation	BPSK(10)
Carrier frequency	2.491 GHz

in mean anomaly). The true anomalies of Satellites 4 and 5 have been optimized with a numerical method and a non-linear cost and constraint function, defined as follows:

- compute all the time windows where GDOP < 5 at the lunar south pole
- discard the windows with a duration of < 6 hours
- enforce that there is at least one valid window per Earth day
- minimize the GDOP on the set of valid windows

The only degrees of freedom of the optimizer are the true anomalies of Satellites 4 and 5. New optimizations may be performed in further studies, with the same procedure, by adding further degrees of freedom combined with mission constraints (e.g., semi-major axis and orbital plane separation).

The assumed characteristics of the navigation payload in charge to transmit the broadcasted signal are summarized in Table 2.

Due to the relatively short distance between the orbits and the Moon's surface, the *effective isotropic radiated power* (EIRP) can be kept quite small compared with Earth GNSS payloads, thus allowing the navigation payload SWaP (size, weight, and power) to be significantly reduced. The selected modulation for this analysis is a simple BPSK(10), similar to GPS L5 or Galileo E5a/E5b, in order to be representative of a future modulation that is compatible with Earth GNSS. The carrier frequency selected for the simulations is S-band (2.491 GHz). There is currently no agreement for navigation specific frequencies as part of the Space Frequency Coordination Group (SFCG, 2019); however, S-band is a good candidate considering the objective to reuse Earth GNSS technology as much as possible and, ideally, avoiding L-band interference with Earth GNSS signals, which could also be used by lunar missions (Delépaut et al., 2020).

The LCNS navigation antenna is assumed nadir-pointing and the LCNS transmission antenna pattern is modeled as isotropic at 0 dBi effective gain within a 30° cone from boresight, effectively fixing the EIRP within 30° from boresight. Clearly, this is a simplification that will have to be further assessed in future work. However, given the low EIRP, it is considered technically achievable. It is important to stress that this aspect will be modified and optimized as a function of the specific LCNS orbit characteristics and the specific service volume selected for the one-way LCNS navigation service.

Finally, different errors have been assumed for the LCNS orbit predictions varying from 5 m to 50 m 1-sigma, while, for the LCNS clock error, a value of 10 m 1-sigma has been considered (which will be identified in Section 4.2 with the variable Σ_{cc}). These errors represent the residual error the user receiver will experience after application of the LCNS navigation message, applying the same concept as Earth GNSS. Studying the current state-of-the-art of orbit determination and time synchronization (ODTS) techniques (Bauer et al., 2017; Exertier et al., 2013; Maier & Baur, 2016; Mazarico et al., 2018; Qin et al., 2019), it is clear that there is not yet

an ultimate approach to achieve accurate LCNS ephemerides when used as part of a real-time broadcast in a lunar navigation system. However, using a combination of existing techniques and technologies, the authors consider that the assumed LCNS orbit and clock errors at maximum *age-of-data* (AOD) are achievable.

The values assumed for the measurement noise matrix (which will be identified in Section 4.2 with the variable Σ_{yy}) are obtained as the sum of the satellite environment noise and the receiver contributions described in Section 4.4. Since the simulation software used for this publication is able to parametrically change the *signal-in-space error* (SISE) contribution and re-assess the final user performance levels, new results will be published when more precise knowledge of the achievable ephemeris accuracy values in lunar orbit is available. In the meantime, a preliminary assessment of performances with this assumed range of accuracy values is provided in Section 5. The concepts of SISE and AOD considered in this publication are in line with the Galileo *Service Definition Document* (SDD; European Commission, 2019).

3.2 | LCNS Proposed Operational Concept and New User Mission CONOPS

As mentioned earlier, the focus of many future lunar missions is the south pole (ISECG, 2020), including setting up a sustainable human presence. Therefore, the proposed orbits have been optimized to cover the region at the cost of lower coverage of the northern hemisphere[2]. With a relatively low number of satellites in the proposed constellation, high service availability everywhere on the lunar surface cannot be achieved. However, lunar missions, being relatively sparse, do not necessarily require navigation services all the time. The majority of the missions would then require navigation services only in specific moments in order to support critical operations.

Maneuvers for orbiters and landers are clear examples: operations are usually performed using Earth infrastructure and require long periods of ground-based ranging to have a good estimation of the satellite orbit (e.g., > 8 hours). Based on the ranging measurements and dynamic models, ground flight dynamic teams compute the expected satellite state vector at the maneuver time and estimate the size of thruster burn in order to achieve the final orbit/trajectory. After the maneuver, the ranging session has to be performed again to confirm the accuracy of the maneuver and assess the need for any correction maneuvers. This process can be quite long (potentially more than one day). An LCNS can provide clear benefits in this sense by offering a much faster positioning solution convergence and a much higher accuracy than with ground-based ranging.

In order to exploit the advantages of LCNS, the user mission analysts have to adapt their mission planning based on LCNS service availability, which is not much different than the current approach used for deep space exploration missions in which mission analysts have to consider the constraints linked to ground station visibility and potential Earth or planet/satellite occultation. This concept of operation is applied also in this paper: the LCNS constellation has been fixed at the beginning of the simulation and the expected availability of the LCNS service has been shared with a mission analyst. The mission timeline has been planned considering LCNS availability, ensuring that major events such as maneuvers have been conducted only when the LCNS service is available.

[2] This initial constellation could be gradually extended with additional satellites in other planes toward a full lunar coverage, adapting to the lunar exploration evolution needs, as explained in Schönfeldt et al. (2020).

4 | LCNS USER EQUIPMENT

4.1 | User Receiver and Antenna

In line with the principles defined in Section 3, the LCNS user receiver has been modeled similarly to a GNSS spaceborne receiver, with standard modular decomposition into a *radio frequency front-end* (RFFE) and digital parts. The antenna gain pattern provided in Figure 2 is in line with currently available high-end GNSS receiver antennas. The RFFE equivalent noise figure has been set to 1 dB, not far from state-of-the-art products available on the market today for space applications. The receiver is assumed to implement standard GNSS acquisition and tracking algorithms. Accordingly, a reasonable threshold of 30 dBHz has been assumed for acquisition and tracking. It is important to note that, for this contribution, the analysis is limited to pseudorange and pseudorange rate observables, so only *delay lock loop* (DLL) and *frequency lock loop* (FLL) have been modeled.

The lander attitude is assumed nominal in the analysis, with the LCNS user antenna always pointing towards zenith considering a Moon-centered, Moon-fixed frame. It is known that the final phase of the lander descent requires attitude changes, however, it is assumed that these changes will be taken into account inside the navigation filter that will be able to propagate the onboard state vector in case of short gaps in LCNS satellite visibility. In addition, multiple antennas could also be installed on the spacecraft to be used in different phases of the landing and potentially also during the surface operations. Since this is not the primary focus of this paper, an analysis including the effects of maneuvers in the navigation filter and the utilization of multiple antennas will be performed and presented in future publications.

The lander avionics will be composed of multiple sensors. Today's lunar lander guidance and navigation (GNC) subunits include visual-based cameras, lidar, radar Doppler altimeters, and inertial units (IMU). Considering that LCNS receivers would not be used in isolation (at least not in the initial phases of the use of the system), it can be safely assumed that the LCNS user receiver can use the benefit of at least two sensors: an IMU and an altimeter (a simplified version of each that is much smaller than the radar Doppler altimeters currently used by landers).

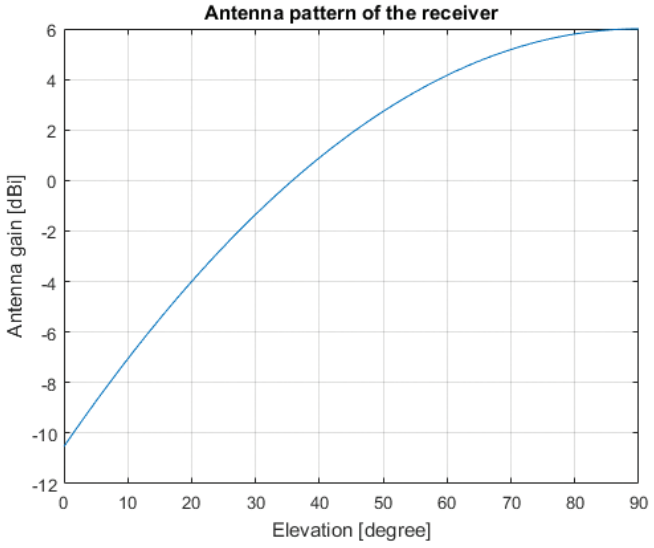

FIGURE 2 Antenna pattern of the receiver

These units are expected to be required by the missions in any case, at least for redundancy.

Within this study, a generic IMU representative of future lunar lander products is considered. The characteristics are similar to the LN200S (Northrop Grumman, 2021) and to the IMU currently under development with the ESA. The altimeter is not modeled in this study as it is not required; as part of a real mission, the altimeter would be able to provide an accurate and precise relative vertical position and velocity to the lunar surface during the final vertical descent, so the GNC function could use the vertical information provided by the altimeter and the horizontal information provided by LCNS to perform its functions. For this reason, we consider that an effective LCNS only needs to provide a horizontal position and velocity solution to the onboard GNC unit.

4.2 | Measurements Model

The adopted measurements include pseudorange p_r^s and pseudorange rate $\dot{p}_r^s$ between a receiver r and each LCNS satellite s in view (described in Section 4.4). The pseudorange rates are assumed to be retrieved through Doppler measurements. The measurement models are:

$$p_r^s = \left\| \boldsymbol{r}_r^s \right\| + dt_r - dt^s + \epsilon_r^s \tag{1}$$

$$\dot{p}_r^s = \left\| \dot{\boldsymbol{r}}_r^s \right\| + \dot{dt}_r - \dot{dt}^s + \varepsilon_r^s \tag{2}$$

where $\boldsymbol{r}_r^s = \boldsymbol{r}^s - \boldsymbol{r}_r$ is the difference between the satellite $\boldsymbol{r}^s$ and receiver $\boldsymbol{r}_r$ position vectors; $\dot{\boldsymbol{r}}_r^s = \dot{\boldsymbol{r}}^s - \dot{\boldsymbol{r}}_r$ is the difference between the satellite $\dot{\boldsymbol{r}}^s$ and receiver $\dot{\boldsymbol{r}}_r$ velocity vectors; dt_r and dt^s are the receiver and satellite clock errors (in meters); $\dot{dt}_r$ and $\dot{dt}^s$ are the receiver and satellite clock error drifts (in meters per second); and ϵ_r^s and ε_r^s are the pseudorange and pseudorange rate noises.

Expanding Equations (1) and (2) as a Taylor's series truncated at the first order about the computed parameters leads to:

$$p_r^s = p_{r,0}^s + \sum \left. \frac{\partial p_r^s}{\partial \boldsymbol{x}_r} \right|_{\boldsymbol{x}_r = \boldsymbol{x}_{r,0}} \Delta \boldsymbol{x}_r + \mathcal{O}\left(\Delta \boldsymbol{x}_r{}^2 \right) \tag{3}$$

$$\dot{p}_r^s = \dot{p}_{r,0}^s + \sum \left. \frac{\partial \dot{p}_r^s}{\partial \boldsymbol{x}_r} \right|_{\boldsymbol{x}_r = \boldsymbol{x}_{r,0}} \Delta \boldsymbol{x}_r + \mathcal{O}\left(\Delta \boldsymbol{x}_r{}^2 \right) \tag{4}$$

where $\boldsymbol{x}_r$ is the assumed state vector, containing the position, velocity, receiver clock error, and receiver clock drift parameters as:

$$\boldsymbol{x}_r = \begin{bmatrix} \boldsymbol{r}_r \\ \dot{\boldsymbol{r}}_r \\ dt_r \\ \dot{dt}_r \end{bmatrix} \tag{5}$$

and $\Delta \boldsymbol{x}_r$ is the increment to the computed parameters of the state vector. The observed minus computed terms therefore become:

$$\Delta p_r^s = p_r^s - p_{r,0}^s = \boldsymbol{u}_r^{s\,T}\left(\boldsymbol{r}^s - \boldsymbol{r}_r\right) + dt_r - dt^s + \epsilon_r^s \tag{6}$$

$$\dot{\Delta} p_r^s = \dot{p}_r^s - \dot{p}_{r,0}^s = \boldsymbol{u}_r^{s\,T}\left(\dot{\boldsymbol{r}}^s - \dot{\boldsymbol{r}}_r\right) + \dot{dt}_r - \dot{dt}^s + \varepsilon_r^s \tag{7}$$

with $\boldsymbol{u}_r^s = \frac{\boldsymbol{r}^s - \boldsymbol{r}_r}{\|\boldsymbol{r}^s - \boldsymbol{r}_r\|} = \frac{\boldsymbol{r}_r^s}{\|\boldsymbol{r}_r^s\|}$. Considering that $\boldsymbol{r}^s$, dt^s, and $\dot{dt}^s$ are computed from the LCNS broadcast ephemeris and corrected as shown in Equation (10), the corrected measurement equation system is hence defined as:

$$E\{\Delta \boldsymbol{y}\} = H \Delta \boldsymbol{x}_r \tag{8}$$

where E is the expectation function, $\Delta \boldsymbol{y}$ is the observed minus computed vector as defined in Equation (10), and H is the design matrix:

$$H = \begin{bmatrix} H_p \\ H_{\dot{p}} \end{bmatrix} = \begin{bmatrix} -\frac{\boldsymbol{r}_r^{1\,T}}{\|\boldsymbol{r}_r^1\|} & \boldsymbol{0}^T & 1 & 0 \\ \vdots & \vdots & \vdots & \vdots \\ -\frac{\boldsymbol{r}_r^{m\,T}}{\|\boldsymbol{r}_r^m\|} & \boldsymbol{0}^T & 1 & 0 \\ -\frac{(\dot{\boldsymbol{r}}_r^1 - (\dot{\boldsymbol{r}}_r^1 \boldsymbol{u}_r^1)\boldsymbol{u}_r^1)^T}{\|\boldsymbol{r}_r^1\|} & -\frac{\boldsymbol{r}_r^{1\,T}}{\|\boldsymbol{r}_r^1\|} & 0\boldsymbol{r}_r^1 & 1 \\ \vdots & \vdots & \vdots & \vdots \\ -\frac{(\dot{\boldsymbol{r}}_r^m - (\dot{\boldsymbol{r}}_r^m \boldsymbol{u}_r^m)\boldsymbol{u}_r^m)^T}{\|\boldsymbol{r}_r^m\|} & -\frac{\boldsymbol{r}_r^{m\,T}}{\|\boldsymbol{r}_r^m\|} & 0\boldsymbol{r}_r^m & 1 \end{bmatrix}$$

$$= \begin{bmatrix} -\frac{\boldsymbol{r}_r^{1\,T}}{\|\boldsymbol{r}_r^1\|} & \boldsymbol{0}^T & 1 & 0 \\ \vdots & \vdots & \vdots & \vdots \\ -\frac{\boldsymbol{r}_r^{m\,T}}{\|\boldsymbol{r}_r^m\|} & \boldsymbol{0}^T & 1 & 0 \\ -\frac{p_{u_r^s}^{\perp}\dot{\boldsymbol{r}}_r^{1\,T}}{\|\boldsymbol{r}_r^1\|} & -\frac{\boldsymbol{r}_r^{1\,T}}{\|\boldsymbol{r}_r^1\|} & 0 & 1 \\ \vdots & \vdots & \vdots & \vdots \\ -\frac{p_{u_r^s}^{\perp}\dot{\boldsymbol{r}}_r^{m\,T}}{\|\boldsymbol{r}_r^m\|} & -\frac{\boldsymbol{r}_r^{m\,T}}{\|\boldsymbol{r}_r^m\|} & 0 & 1 \end{bmatrix} \tag{9}$$

The last equality in Equation (9) derives from the fact that $\dot{\boldsymbol{r}}_r^s - (\dot{\boldsymbol{r}}_r^s \boldsymbol{u}_r^s)\boldsymbol{u}_r^s$ is the projection of $\dot{\boldsymbol{r}}_r^s$ on the subspace orthogonal to $\boldsymbol{u}_r^s$, $p_{u_r^s}^{\perp}$, as also reported in Vincent et al. (2020). Differently from the present contribution, the dependence on the observer's velocity is dropped because in the cited research the observer is stationary, as pointed out in Vincent et al. (2019). Equation (9) is in line with the approach provided by Psiaki (2021).

Collecting all the measurements p_r^s and $\dot{p}_r^s$, respectively, in the m-vectors $\boldsymbol{p}$ and $\dot{\boldsymbol{p}}$, the transformation matrix $T_{cor}(i)$ allows the derivation of the $2m$-vector of corrected observations $\Delta \boldsymbol{y}(i)$ (observed minus computed) as:

$$\Delta \boldsymbol{y}(i) = T_{cor}(i) \begin{bmatrix} \boldsymbol{p} \\ \dot{\boldsymbol{p}} \\ \boldsymbol{r}^S \\ \dot{\boldsymbol{r}}^S \\ dt^S \\ \dot{dt}^S \end{bmatrix}_{(i)} \tag{10}$$

where, for each epoch i:

- $T_{cor}(i)$ is the transformation matrix, defined as:

$$T_{cor}(i) = \begin{bmatrix} I_m & 0 & -U_r^S(i) & 0 & I_m & 0 \\ 0 & I_m & 0 & -U_r^S(i) & 0 & I_m \end{bmatrix} \tag{11}$$

- m is the number of satellites in view
- $\boldsymbol{r}^s$ is the $3m$-vector with LCNS satellite positions
- $\dot{\boldsymbol{r}}^s$ is the $3m$-vector with LCNS satellite velocities
- dt^s is the m-vector with LCNS satellite clock bias
- $\dot{dt}^s$ is the m-vector with LCNS satellite clock drift
- $U_r^S(i) = \oplus_{s=1}^{m} \boldsymbol{u}_r^{s^T}$ is the geometry matrix containing the unit vectors $\boldsymbol{u}_r^s$ with the directions toward the LCNS satellites being $\oplus$ the direct sum of matrices and where $I_{(\cdot)} = \text{diag}(1,\ldots,1)$.

Equation (10) is not how real measurement residuals are computed, which is usually performed by differencing the observed minus the non-linear models; rather, it is just providing a way to derive the measurement covariance. The covariance matrix $R_{\Delta y \Delta y}$ for the corrected measurements $\Delta \boldsymbol{y}(i)$, indicating the user navigation accuracy, accounts for two distinct contributions:

- An observation covariance matrix, Σ_{yy} (see Section 3.1), associated with the LCNS measurements $\boldsymbol{y}(i) = \begin{bmatrix} \boldsymbol{p} \\ \dot{\boldsymbol{p}} \end{bmatrix}$ (the variances of distinct measurements are uncorrelated), accounting for the user equipment error (UEE), which depends on the capabilities and environment of the user's navigation device; and
- a covariance matrix associated to the LCNS ephemeris, Σ_{cc} (see Section 3.1), which is propagated to the variance of the measurements to which the corrections are applied and whose performance is dependent on the system provider.

It is therefore computed as:

$$\Sigma_{\Delta y \Delta y} = T_{cor} \begin{bmatrix} \Sigma_{yy} & 0 \\ 0 & \Sigma_{cc} \end{bmatrix} T_{cor}^T \tag{12}$$

The sub-matrix Σ_{yy}, written as:

$$\Sigma_{yy} = \begin{bmatrix} \Sigma_{pp} & 0 \\ 0 & \Sigma_{\dot{p}\dot{p}} \end{bmatrix} \tag{13}$$

is diagonal, as it is assumed that there is no correlation between the observations.

4.3 | Positioning Algorithm

The position determination process is carried out using an extended Kalman filter (EKF), similar to Earth-based GNSS positioning. The estimation is kinematic and not dynamic, which means it does not embed orbit propagation dynamics which would require advanced modeling. Using such a kinematic approach is a conservative assumption, as precision could only be enhanced by adding the dynamic part. Several references already exist on this topic and the reader is redirected to them for further details on EKF (Brown & Hwang, 2012). The EKF mathematical description is summarized in the following equations, noting that, as this is a variance-covariance analysis, the state estimation based on EKF equations is not needed and thus will not be detailed.

The filter initial state covariance matrix P is initialized through a weighted least squares (WLS), obtaining P_0. The predicted state covariance matrix is computed as:

$$P_k^- = F_{k-1,k} P_{k-1} F_{k-1,k}^T + \Gamma Q_{k-1} \Gamma^T \tag{14}$$

where k is the current epoch, $k-1$ the previous epoch, $F_{k-1,k}$ is the state transition matrix (STM), Q_{k-1} is the process noise covariance matrix, Γ is the process noise transition matrix, and the superscript "$\cdot^-$" means *predicted*. The measurement update step is performed as:

$$K_k = P_k^- H_k^T \left(H_k P_k^- H_k^T + \Sigma_k \right)^{-1} \tag{15}$$

$$P_k = \left(I - K_k H_k \right) P_k^- \left(I - K_k H_k \right)^T + K_k \Sigma_k K_k^T \tag{16}$$

where Σ_k (referred in the previous section as $\Sigma_{\Delta y \Delta y}$, where now the subscript has been changed to k to indicate a temporal dependence) is the measurement covariance matrix. The Bucy-Joseph formulation has been used to compute the state covariance matrix, which is preferred for such numerical applications as it ensures that P_k is a symmetric matrix. For this analysis, the filter has been set to use LCNS signals only for estimation of both position and velocity.

4.3.1 | *Prediction Model*

The prediction model and mechanization of the filter is handled by the state transition and process noise matrices, F, Q, and Γ, defined as:

$$F = \begin{bmatrix} I_{3\times3} & I_{3\times3} \cdot \Delta T & & \\ & I_{3\times3} & & \\ & & 1 & \Delta T \\ & & & 1 \end{bmatrix} \tag{17}$$

$$Q = \begin{bmatrix} I_{3\times3} \cdot \sigma_p^2 & & & \\ & I_{3\times3} \cdot \sigma_v^2 & & \\ & & \sigma_{\delta t}^2 & \\ & & & \sigma_{\dot{\delta} t}^2 \end{bmatrix} \tag{18}$$

$$\Gamma = \begin{bmatrix} I_{3\times3}\cdot\Delta T & & & \\ & I_{3\times3}\cdot\Delta T & & \\ & & \Delta T & \\ & & & \Delta T \end{bmatrix} \tag{19}$$

where ΔT is the measurement rate. A uniform motion performed by the spacecraft is assumed and, therefore, the position prediction is based on the velocity estimation at $k-1$ epoch. In reality, the spacecraft motion is non-uniform in nature and, therefore, some uncertainty is added to the prediction step by the Q matrix, which includes the process noise of position and velocity. The process noise plays a significant role in the final precision and convergence time of the filter. Preliminary analyses considering the contribution from the selected IMU have shown that 1 cm/s velocity prediction (1–10 s) is achievable. Therefore, for this assessment, 0.01 m position process noise and 0.01 m/s velocity process noise are assumed. Note that this is a conservative approach; the authors plan to perform further sensitivity analyses of the process noise and a complete LCNS/IMU fusion positioning filtering as part of future studies.

4.4 | Measurement Precision

As introduced in Section 3.1, the LCNS signal considered for this publication is a BPSK(10), so the receiver measurement noise is modeled using the same methodology that has been adopted for Earth GNSS, considering that the pseudorange jitter assumes a *delay lock loop* (DLL), while Doppler measurements assume a *frequency lock loop* (FLL). The precision is retrieved using Equations (20) and (21) derived from Kaplan and Hegarty (2006), as well as the parameters described in Table 3.

$$\sigma_{DLL} = \lambda_C \sqrt{\frac{B_L d}{2\cdot CN0}\left(1+\frac{1}{T_i\cdot CN0}\right)} \tag{20}$$

$$\sigma_{FLL} = \frac{\lambda_L}{2\pi T_i}\sqrt{\frac{4FB_L}{CN0}\left(1+\frac{1}{T_i\cdot CN0}\right)} \tag{21}$$

For carrier-to-noise ratio (C/N_0) estimation, the complete link budgets from satellites to receiver have been simulated using a satellite toolkit, based on the user receiver and antenna parameters described in Section 4.1. The simulator is similar

TABLE 3
DLL and FLL Track Loop Parameters

Parameters	LCNS
Loop bandwidth (BL)	0.5 Hz
Coherent integration (Ti)	20 ms
Early-late spacing (d)	1 chip
Wavelength (lambda)	14.28 cm
Chip length (lambda c)	29.305 m
Factor (F) for high/low C/N_0	1 or 2

TABLE 4
Simulation Parameters Summary

Simulation Parameters	LCNS
Constellation used	5 ELFO
Orbit propagation	STK HPOP
LCNS SISE (1 sigma)	Position (x, y, z): (15, 15, 15) m (1D) Velocity (x, y, z): (0.15, 0.15, 0.15) m/s (1D) Clock : 10 m Clock drift : 0.1 m/s
C/N_0 acquisition and tracking sensitivity	30 dBHz
Measurements	Pseudorange, pseudorange-rate (Doppler)
Measurement rate	1 Hz
Measurement noise	Based on C/No
Motion model	Uniform, velocity-based
Motion process noise	Position σ_p (x, y, z): (0.01, 0.01, 0.01) $m/\sqrt{s}$ Velocity σ_v (x, y, z): (0.01, 0.01, 0.01) $m/s/\sqrt{s}$ Clock $\sigma_{\delta t}$: 100 $m/\sqrt{s}$ Clock drift $\sigma_{\dot{\delta t}}$: 1 $m/s/\sqrt{s}$
Initial precision	Position (x, y, z): 1 km 3D 1-sigma Velocity (x, y, z): 100 m/s 3D 1-sigma Clock: 100 m 1-sigma Clock drift: 1 m/s 1-sigma

to the one used in Delépaut et al. (2020). Based on the link budget, the C/N_0 reaches up to 55 dBHz during the LLO simulation; however, in the majority of the cases, it stays between 30 dBHz and 40 dBHz.

The measurement noise matrix Σ_{YY} is composed of the pseudorange and the pseudorange-rate noise matrices Σ_{PP} and $\Sigma_{\dot{P}\dot{P}}$ defined as:

$$\Sigma_{PP} = diag\left(\sigma^2_{DLL,1},\ldots,\sigma^2_{DLL,m}\right) \tag{22}$$

$$\Sigma_{\dot{P}\dot{P}} = diag\left(\sigma^2_{FLL,1},\ldots,\sigma^2_{FLL,m}\right) \tag{23}$$

$$\Sigma_{yy} = \begin{bmatrix} \Sigma_{pp} & 0 \\ 0 & \Sigma_{\dot{p}\dot{p}} \end{bmatrix} \tag{24}$$

A summary of the parameters used in the simulation is provided in Table 4.

5 | PERFORMANCE ANALYSIS

5.1 | Low Lunar Orbit Phase Performance

The proposed analysis would be performed over 24 hours, from June 11, 2026, 15:00:00 to June 12, 2026, 15:00:00, while the spacecraft is in LLO at an altitude of around 100 km. This scenario length is representative of the time required for the flight dynamic team to compute the orbit based on ground measurements and

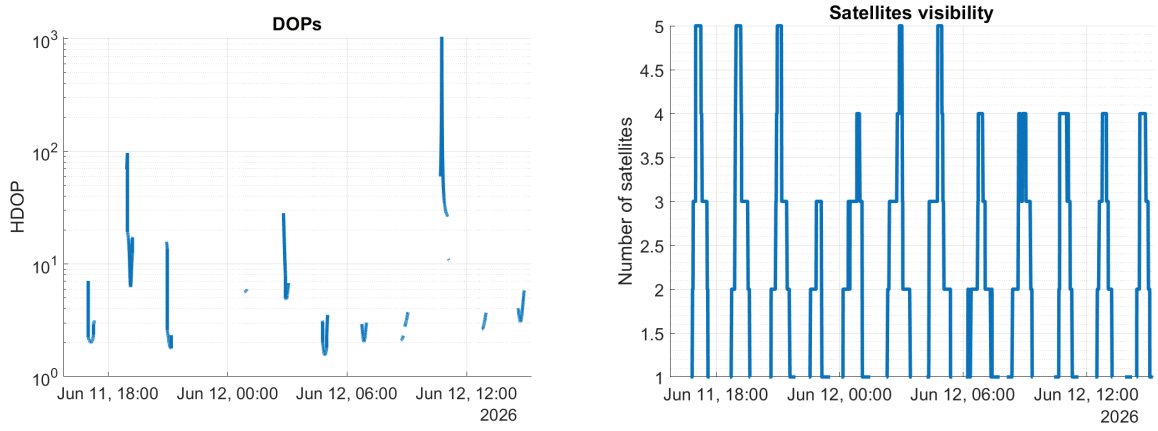

FIGURE 3 LLO precision analysis (24 hours): dilution of precision (left), and number of visible satellites (right)

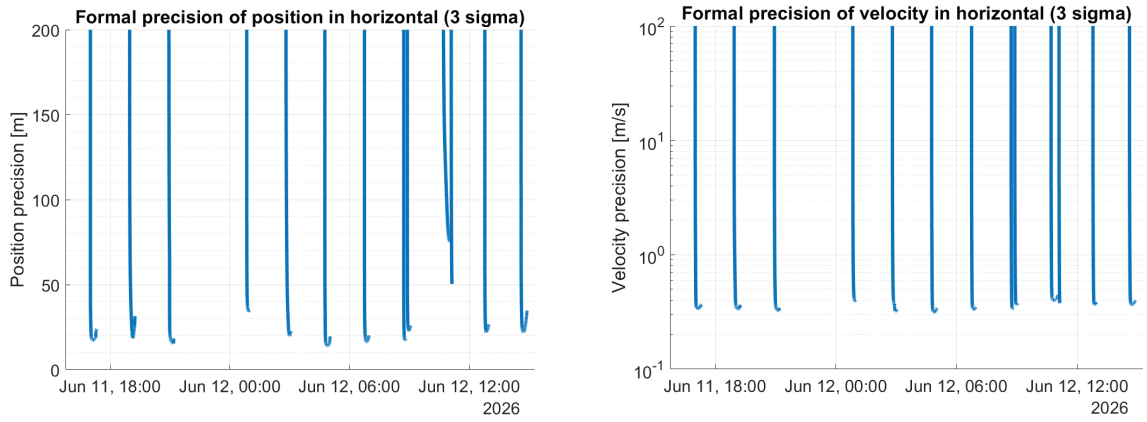

FIGURE 4 LLO precision analysis (24 hours): precision (3-sigma) of position (left), and precision of velocity (right)

then compute the maneuvers for the final descent. Due to the specific orbit and the selected period, the Moon would occult the satellite for some of the time.

In the same way, due to the specific ELFO orbit, which privileges the lunar south pole, at some periods the LCNS receiver would experience gaps in the reception of LCNS signals (see Figures 3 and 4) leading to the unavailability of a solution in precision analysis when the number of visible satellites is below four. This is a conservative assumption, since in the case that a dynamic model is implemented within the LCNS receiver navigation filter, the orbits and hence its precision could be properly propagated during signal reception gaps. Specific sequential dynamic filters for lunar orbit real-time determination are currently under development at the ESA and could be used within the LCNS receiver. Even without a dynamic model, the precision would converge to a reasonable level within a few minutes, showing the resilience of the system.

This analysis shows that, given the assumptions presented in the previous sections, a spacecraft in LLO with an LCNS receiver could reach a precision below 30 m (3-sigma) when enough LCNS satellites are visible. Figures 5 and 6 show the performances over a period of four hours, covering two orbits of the LLO satellite. As explained earlier, the state vector estimated onboard can be propagated with orbital dynamic models during the visibility gaps, maximizing the onboard autonomy with respect to ground contacts.

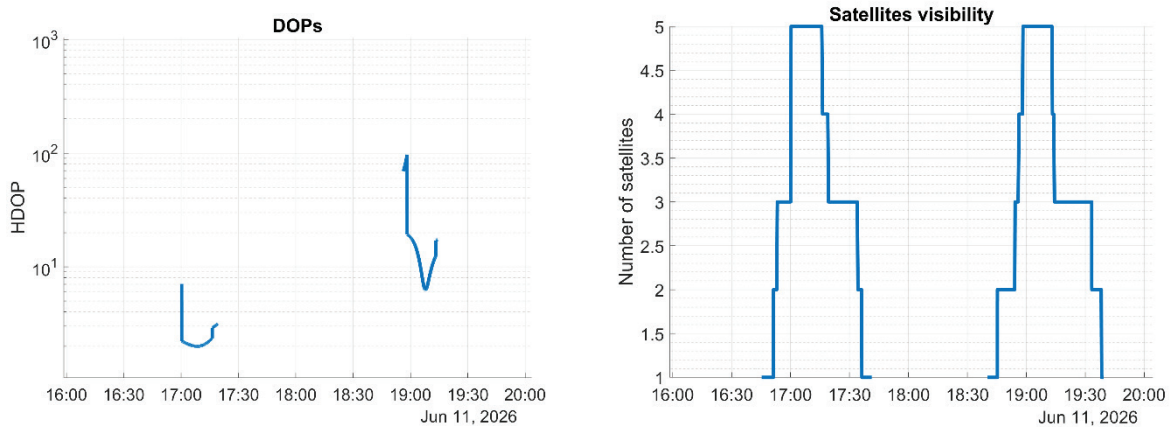

FIGURE 5 LLO precision analysis zoomed over two orbits (4 hours): dilution of precision (left), and number of visible satellites (right)

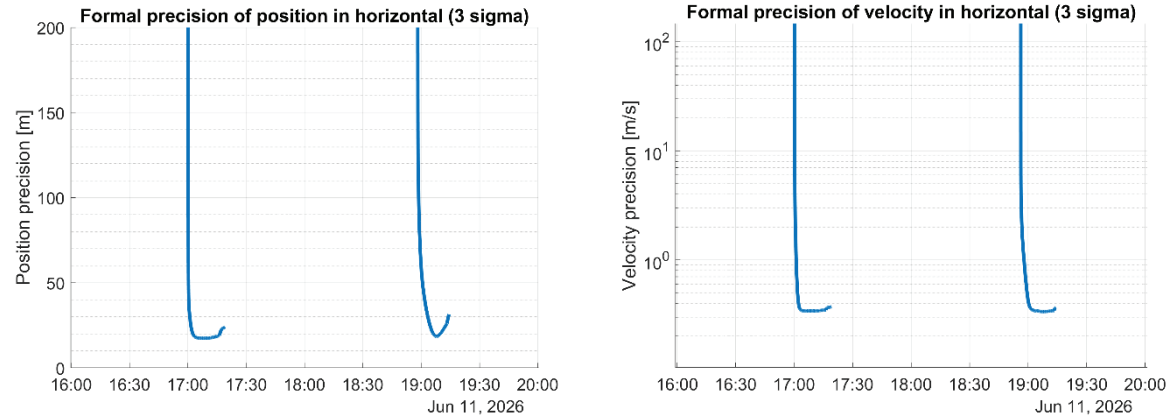

FIGURE 6 LLO precision analysis zoomed over two orbits (4 hours): precision (3-sigma) of position (left), and precision of velocity (right)

The increased onboard autonomy has a direct impact on the cost of the mission, as almost-continuous Earth ground-based measurements over several days are usually needed to achieve convergence of the orbit determination solution with a much poorer precision compared to LCNS-based solutions. The typical orbit determination cycle consists of 48 hours of tracking and radiometric measurements, followed by 48 additional hours in which the ground-based team is devoted to processing the solution as well as planning and uploading the maneuvers. A lunar mission based on traditional Earth ground-based measurements would then require a minimum loitering time of four days in LLO before landing.

The precision of ground-based orbit determination is driven by several parameters, such as the measurement availability and the measurement and dynamic model quality. It is common practice to quantify the latter in terms of unmodeled accelerations: a spacecraft is called *noisy* when the dynamic model used for its state vector prediction is not able to accurately model all of the applicable forces, while a spacecraft is *quiet* when the dynamic model used on ground is very accurate. For the EL3 mission, the preliminary expected 3-sigma precision in LLO after the four-day process described earlier is between 800 m and 11 km position and 0.8 m/s and 2 m/s velocity, depending on the unmodeled accelerations and assuming continuous availability of an ESTRACK ground station with range and Doppler

TABLE 5
Ground-Based Navigation Analysis Assumptions

Parameter	Value
Ground station position bias	30 cm spherical
Range observation bias	10 m
Range random noise component	2 m
Doppler random noise component	0.3 mm/s for 60 s count time
Min. spacecraft elevation	15°

measurements. This preliminary navigation analysis has been performed with an ESA/ESOC software, using the assumptions reported in Table 5.

A precision-level comparable to LCNS-based navigation could be achieved also with DTE-based techniques by reducing the ground processing time to 12 hours prior to maneuvers. This reduction would allow a shorter propagation of the orbit determination solution in order to reduce the error induced by the force mismodeling. However, this approach would increase the effort and the size of the ground-based team, with significant impact on the mission cost and the positioning precision would not be reduced below some tens of meters.

In order to further reduce the overall loitering time, the duration of the measurement campaign could be reduced instead (e.g., to 24 hours), but the quality of the orbit determination could be hindered by the lower number of available measurements. The advantage of an LCNS-based orbit determination is then apparent in terms of precision, reduction of the mission timeline, and onboard availability of the state estimation.

5.2 | Final Descent Performance

The targeted site of the descent phase is located near the south pole of the Moon, on the far side. No direct link with the Earth is available during this phase, so the spacecraft would rely on a closed loop onboard navigation process to attempt to reach the planned landing site. As seen in Section 5.1, the visibility of LCNS satellites on the lunar south pole varies with time, however, considering that the ELFO orbits are very stable, the user mission can predict the expected LCNS satellite visibility well in advance along with the related expected performance levels. As explained in Section 3.2, the visibility of LCNS over the landing region has been pre-computed and provided to the mission analysts, who then selected the best window for landing operation considering both mission and LCNS constraints. The use of an altimeter that would give the direct height under the spacecraft in the final approach is assumed.

Similar to Earth GNSS, precise height is difficult to achieve with satellite positioning only, especially with so few satellites in view. Moreover, a satellite system will only give the ellipsoidal height, not the actual height on the surface, which could only be used with very precise digital elevation models (DEMs) of the landing site. Moreover, it is expected that landers will be equipped with altimeters and, therefore, this analysis focuses on horizontal precision only.

As presented in Section 2, the first maneuver to initiate the descent would be performed half an orbit before landing over the lunar north pole. From that point onward, the altitude would slowly decrease. Figure 7 shows the altitude with

respect to the lunar surface for the final minutes before the last landing maneuver that would initiate the actual descent.

As mentioned previously, the trajectory has been selected to ensure the best geometry during the most critical phase of the descent. Figure 8 shows how the number of satellites visible by the receiver would increase over time. The computations of the navigation solution starts as soon as four satellites are visible (around 16:29 in Figure 8), however the filter has some difficulties to converge, because no sufficient redundancy is present and the geometry is not optimal, as highlighted by the higher DOP present in Figure 8. However, even with suboptimal geometry, the filter would still achieve a horizontal precision of 35 m (3-sigma). Once the fifth satellite is received, the filter would start converging, reaching a horizontal precision of 20 m (3-sigma) in one minute, before the final maneuvers would be performed after 16:34 (see the change of altitude in Figure 7). The filter would continue to improve the horizontal position estimation during the final landing phase,

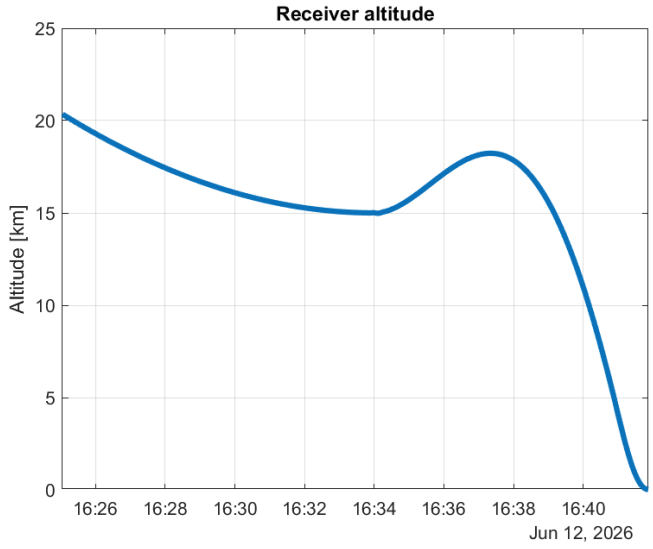

FIGURE 7 Altitude with respect to the lunar surface during landing

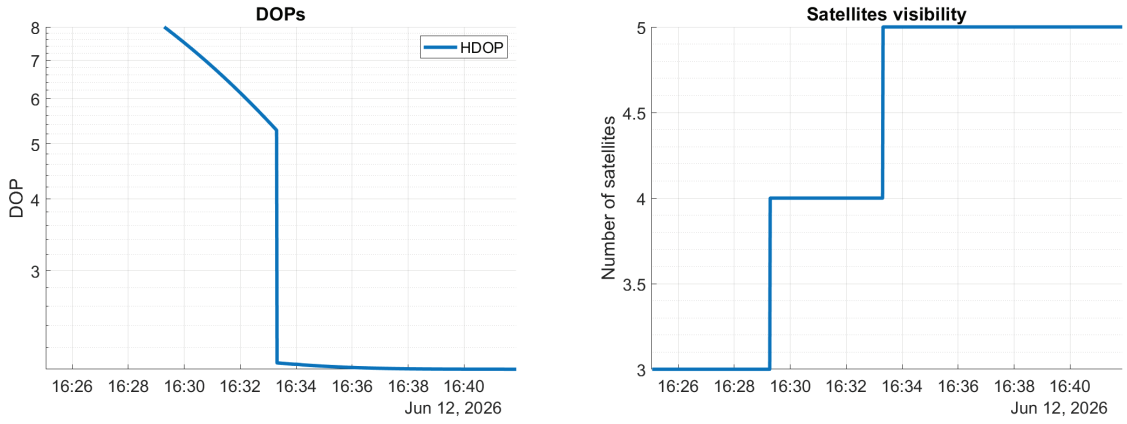

FIGURE 8 Landing precision analysis: dilution of precision (left) and number of visible satellites (right)

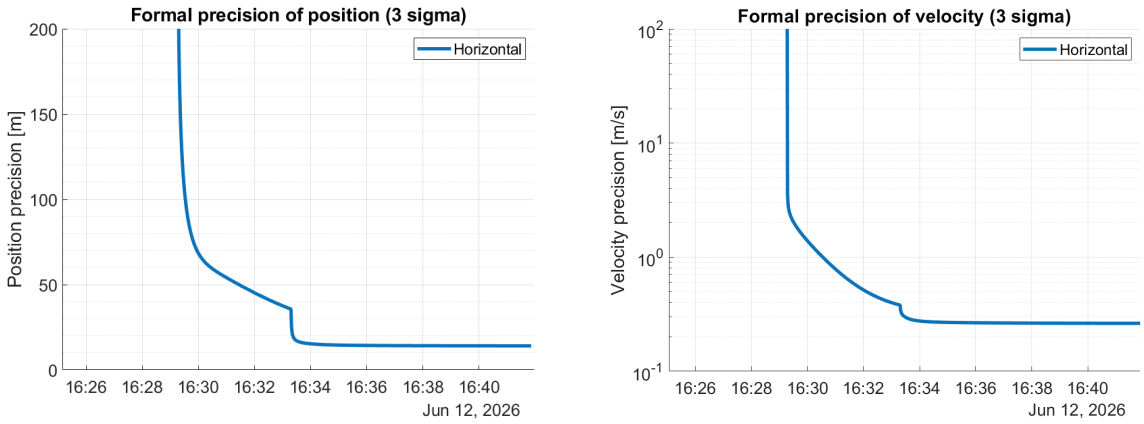

FIGURE 9 Landing precision (3-sigma) analysis: precision of position (left) and precision of velocity (right)

TABLE 6
Statistics of Position and Velocity Precision at Landing Location

	Position precision (3-sigma)	Velocity precision (3-sigma)
Horizontal (4 satellites)	19.6 m	0.28 m/s
Horizontal (5 satellites)	14.1 m	0.26 m/s

reaching a final position precision of 14.1 m (3-sigma) and velocity precision of 0.26 m/s (3-sigma), as seen in Figure 9.

The simulation of the final descent considers a worst-case scenario for the initial position, velocity, and clock precision as shown in Table 4. The results presented in Section 5.1 show that an LCNS can provide much better levels of performance in LLO, however it was decided to be conservative and simulate a worst-case scenario. The use of an LCNS in LLO is expected to reduce the convergence time of the filter, providing a better performance earlier in the final descent.

A summary of the position and velocity precision considering four or five LCNS satellites is provided in Table 6. The best levels of performance would be clearly achieved with five satellites, however it is possible to be compliant with the *Global Exploration Roadmap* requirement even with four satellites.

The results presented so far assume 15-m orbit and 10-m clock ODTS errors (1-sigma) as presented in Section 3.1. It is currently unclear if the LCNS orbit determination and time synchronization capability would allow the achievement of these SISE values, so a parametric sensitivity analysis has been performed. The subsequent results are presented in Figure 10, in which the position precision is plotted as a function of different LCNS orbit and clock errors. As expected, the satellite precision would worsen with increased LCNS orbit and clock errors. Yet, even for the most conservative 50-m orbit error assumption, the actual achievable values are still within the requirement expressed in the *Global Exploration Roadmap Critical Technology Needs* (ISECG, 2019) with some margin, being within 90 m 3-sigma at the final landing location (GER-018).

Even if this contribution focuses on precision and not directly on accuracy, due to the aforementioned margin, the contribution of biases in the final position solution should not lead to a non-compliance to the GER-018 requirement. Further analysis including system and receiver biases will be performed in future studies.

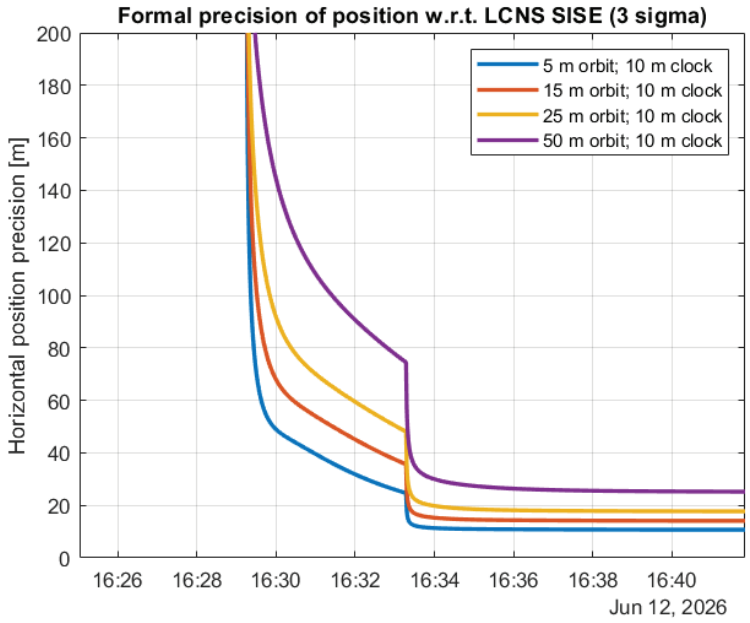

FIGURE 10 Formal precision of position (3-sigma) with regard to LCNS SISE

6 | CONCLUSION

Landing on the Moon is still considered a complex task, notably if the target landing location is on the far side of the Moon. The standard approach for spacecraft navigation currently, based on the use of radiometric measurements from Earth, requires significant operational effort, including loitering for several days in low lunar orbit to achieve a sufficiently accurate orbit determination to start the final descent (shorter periods can be considered, but only with higher complexity and cost). The requirements expressed as part of the *Global Exploration Roadmap Critical Technology Needs* (ISECG, 2019) could be met with current state-of-the-art visual-based navigation technology such as the one used for the recent Mars landing, but only with a relatively expensive cost and heavy equipment dedicated to the landing phase, which is only partially reusable after touch down.

This study has shown that a dedicated LCNS system consisting of five satellites would allow a spacecraft equipped with an LCNS receiver to compute its position, velocity, and time in real-time onboard with a short convergence time and high precision reaching performance levels that are similar, and in some cases, better than ground-based orbit determination. In the landing phase, horizontal landing precision below 30 m 3-sigma is obtained with orbit and clock contributions to SISE of around 50 m and 10 m, respectively. Horizontal landing precision below 10 meters is achievable with SISE orbit and clock below 15 m and 10 m, respectively, which could enable completely new types of missions and be well within the *Global Exploration Roadmap* landing requirements. The analysis in this contribution shows that LCNS receivers can be seen as redundant sensors to visual-based navigation in the initial phase of LCNS deployment and, later, might even become an alternative solution. The aim of the Moonlight/LCNS navigation service is to move the complexity and cost (both development and operational) of the navigation function from the user missions to a lunar system available to all users. This is considered to be more cost-effective in the long-term considering the large number of missions planned in the future and

the objective to achieve a long-term and sustainable human and robotic presence on the Moon.

Upcoming missions such as ESA's EL3 (European Large Logistics Lander) require dedicated sensors for absolute navigation with respect to the Moon's surface, a radar Doppler altimeter for velocity measurements, and lidar for hazard detection. The lander performance simulated in this paper shows that an LCNS could provide redundancy to the well-established sensors and eventually replace some of them, leading to significant savings in terms of weight, mass, power consumption, and overall costs. An LCNS would allow us to target safely and repeatedly the same area on the lunar surface within 30 m, limiting hazard detection and hazard avoidance maneuvers. The much faster state estimation convergence to the required precision would significantly reduce the necessary ground operational effort, increasing the flexibility in the final descent phase. In addition, it could also enable rapid access to the surface, for example for human emergency cargo delivery.

Furthermore, the availability of an LCNS would simplify lunar mission design right from the early stages, reducing the dependency on ground-based mission analysis and eventually decoupling the navigation problem from the mission analysis task. Phase 0 and pre-phase A studies could already benefit from the working assumption of having the spacecraft state available after a given time frame and with a given accuracy.

From 2021 through 2022, the LCNS/Moonlight constellation and concept will be defined as part of the ESA's dedicated Phase A/B1 studies. This will, in turn, define the specific LCNS constellations proposed for implementation, which may differ from the one presented in this publication. Yet, the concept and conclusions described in this contribution remain valid and show how a dedicated lunar radio navigation system may become a key enabler for future lunar missions, covering the requirements expressed in the global space exploration roadmap. This is the firm conviction of the authors of this paper.

ACKNOWLEDGMENTS

The authors would like to thank the anonymous reviewers for the very valuable comments received.

REFERENCES

Barton, G. H., Shepperd, S. W., & Brand, T. J. (1993). Proposed autonomous lunar navigation system. *Astrodynamics 1993*, 1717–1736.

Bauer, S., Hussmann, H., Oberst, J., Dirkx, D., Mao, D., Neumann, G. A., Mazarico, E., Torrence, M. H., McGarry, J. F., Smith, D. E., & Zuber, M. T. (2017). Analysis of one-way laser ranging data to LRO, time transfer and clock characterization. *Icarus, 283*, 38–54. https://doi.org/10.1016/j.icarus.2016.09.026

Brown, R. G., & Hwang, P. Y. (2012). *Introduction to random signals and applied Kalman filtering* (4th ed.). John Wiley & Sons.

Capuano, V., Blunt, P., Botteron, C., Tian, J., Leclère, J., Wang, Y., Basile, F., & Farine, P.-A. (2016). Standalone GPS L1 C/A receiver for lunar missions. *Sensors, 16*(3), 347–368. https://doi.org/10.3390/s16030347

Carpenter, J. R., Folta, D. C., Moreau, M. C., & Quinn, D. A. (2004). Libration point navigation concepts supporting the vision for space exploration. *AIAA/AAS Astrodynamics Specialist Conference and Exhibit,* Providence, RI. https://doi.org/10.2514/6.2004-4747

Cheetham, B. (2020). Cislunar Autonomous Positioning System Technology Operations and Navigation Experiment (CAPSTONE). *ASCEND 2020.* Aerospace Research Central. https://doi.org/10.2514/6.2020-4140

Chen, H., Liu, L., Meng, Y., Xu, Z., Long, L., & Liu, J. (2017). Preliminary mission design and analysis of a lunar far-side positioning CubeSat mission. *26th International Symposium on Space Flight Dynamics,* Matsuyama, Japan. https://issfd.org/ISSFD_2017/paper/ISTS-2017-d-160__ISSFD-2017-160.pdf

Circi, C., Romagnoli, D., & Fumenti, F. (2014). Halo orbit dynamics and properties for a lunar global positioning system design. *Monthly Notices of the Royal Astronomical Society*, *442*(4), 3511–3527. https://doi.org/10.1093/mnras/stu1085

Delépaut, A., Giordano, P., Ventura-Traveset, J., Blonski, D., Schönfeldt, M., Schoonejans, P., Aziz, S., & Walker, R. (2020). Use of GNSS for lunar missions and plans for lunar in-orbit development. *Advances in Space Research, 66*(12), 2739–2756. https://doi.org/10.1016/j.asr.2020.05.018

Delépaut, A., Schönfeldt, M., Giordano, P., Blonski, D., Sarnadas, R., Ries, L., & Ventura-Travaset, J. (2019). A system study for cislunar radio navigation leveraging the use of realistic Galileo and GPS signals. *Proc. of the 32nd International Technical Meeting of the Satellite Division of the Institute of Navigation (ION GNSS+ 2019)*, Miami, FL, 1199–1219. https://doi.org/10.33012/2019.17084

Euroconsult. (2020). *Prospects for space exploration.* Euroconsult.

European Commission. (2019). *European GNSS (Galileo) open service - service definition document (SDD)*. https://www.gsc-europa.eu/sites/default/files/sites/all/files/Galileo-OS-SDD_v1.1.pdf

European Space Agency (ESA). (2019). *To the Moon – down south*. https://www.esa.int/Science_Exploration/Human_and_Robotic_Exploration/Exploration/To_the_Moon_down_south

European Space Agency (ESA). (2020). *Moonlight: connecting Earth with the Moon*. https://www.esa.int/ESA_Multimedia/Videos/2020/11/Moonlight_connecting_Earth_with_the_Moon/(lang)

European Space Agency (ESA). (2021). *European large logistics lander*. https://www.esa.int/Science_Exploration/Human_and_Robotic_Exploration/Exploration/European_Large_Logistics_Lander

Exertier, P., Samain, E., Courde, C., Martin, N., Torre, J. -M., Oneto, J. -L., Laas-Bourez Geoazur, M., Guillemot, Ph., & Léon, S. (2013). T2L2: Five years in space. *2013 Joint European Frequency and Time Forum & International Frequency Control Symposium (EFTF/IFC)*, Prague, Czech Republic, 632–635. https://doi.org/10.1109/EFTF-IFC.2013.6702281

Farquhar, R. W. (1971). *The utilization of halo orbits in advanced lunar operations.* National Aeronautics and Space Administration. https://www.lpi.usra.edu/lunar/documents/NASA%20TN%20D-6365.pdf

Gao, Y.-X., Ge, Y.-M., Ma, L.-X., Hu, Y.-Q., & Chen, Y.-X. (2019). Optimization design of configuration and layout for Queqiao relay satellite. *Advances in Astronautics Science and Technology*, 2, 33–38. https://doi.org/10.1007/s42423-019-00034-0

Guptan, M. (2019). How did Chandrayaan 2 fail? ISRO finally has the answer. *The Week*. https://www.theweek.in/news/sci-tech/2019/11/16/how-did-chandrayaan-2-fail-isro-answer.html

Halon, E. (2019). SpaceIL reveals preliminary reasons behind Beresheet crash. *The Jerusalem Post*. https://www.jpost.com/israel-news/spaceil-reveals-preliminary-reasons-behind-beresheet-crash-587117

International Space Exploration Coordination Group (ISECG). (2019). *Global exploration roadmap critical technology needs.* International Space Exploration Coordination Group Technology Working Group. https://www.globalspaceexploration.org/wp-content/uploads/2019/12/2019_GER_Technologies_Portfolio_ver.IR-2019.12.13.pdf

International Space Exploration Coordination Group (ISECG). (2020). *Global exploration roadmap: Lunar surface exploration scenario update (Supplement August 2020).* https://www.globalspaceexploration.org/: https://www.globalspaceexploration.org/wp-content/uploads/2020/08/GER_2020_supplement.pdf

Israel, D. J., Mauldin, K. D., Roberts, C. J., Mitchell, J. W., Pulkkinen, A. A., Cooper, L. D., Johnson, M. A., Christe, S. D., & Gramling, C. J. (2020). LunaNet: A flexible and extensible lunar exploration communications and navigation Infrastructure. *2020 IEEE Aerospace Conference,* Big Sky, MT. https://doi.org/10.1109/AERO47225.2020.9172509

Johnson, A., Aaron, S., Chang, J., Cheng, Y., Montgomery, J., Mohan, Schroeder, S. Tweddle, B., Trawny, N., & Zheng, J. (2017). The lander vision system for Mars 2020 entry descent and landing. *AAS Guidance Navigation and Control Conference.* Breckenridge, CO. http://hdl.handle.net/2014/46186

Kaplan, E. D., & Hegarty, C. J. (2006). *Understanding GPS/GNSS: Principles and applications.* Artech House.

MacNicol, J. H., & Raquet, J. M. (2002). A study of satellite navigation, dilution of precision, and positioning techniques for use on and around the Moon. *Proc. of the 58th Annual Meeting of The Institute of Navigation and CIGTF 21st Guidance Test Symposium*, Albuquerque, NM, 506–515. https://www.ion.org/publications/abstract.cfm?articleID=982

Maier, A., & Baur, O. (2016). Orbit determination and gravity field recovery from Doppler tracking data to the Lunar Reconnaissance Orbiter. *Planetary and Space Science, 122*, 94–100. https://doi.org/10.1016/j.pss.2016.01.014

Mazarico, E., Neumann, G. A., Barker, M. K., Goossens, S., Smith, D. E., & Zuber, M. T. (2018). Orbit determination of the Lunar Reconnaissance Orbiter: Status after seven years. *Planetary and Space Science, 162*, 2–19. https://doi.org/10.1016/j.pss.2017.10.004

Miller, J. (2019). *Planetary spacecraft navigation.* Springer International Publishing. https://doi.org/10.1007/978-3-319-78916-3

National Aeronautics and Space Administration (NASA). (2020). *NASA names companies to develop human landers for Artemis moon missions*. https://www.nasa.gov/press-release/nasa-names-companies-to-develop-human-landers-for-artemis-moon-missions

National Aeronautics and Space Administration (NASA). (2021). *NASA Artemis*. https://www.nasa.gov/specials/artemis

Northrop Grumman. (2021). *LN-200S inertial measurement unit*. https://www.northropgrumman.com/what-we-do/ln-200s-inertial-measurement-unit

Parker, J. S., Smith, J., Forsman, A., Rabotin, C., Cain, C., & Cheetham, B. (2019). The Cislunar Autonomous Positioning System, CAPS. *Advances in the Astronautical Sciences Guidance, Navigation and Control 2019, 169*.

Psiaki, M. (2021). Navigation using carrier Doppler shift from a LEO constellation: TRANSIT on steroids. *NAVIGATION*, 68(3), 621– 641. https://doi.org/10.1002/navi.438

Qin, S., Huang, Y., Li, P., Shan, Q., Fan, M., Hu, X., & Wang, G. (2019). Orbit and tracking data evaluation of Chang'E-4 relay satellite. *Advances in Space Research, 64(4)*, 836–846. https://doi.org/10.1016/j.asr.2019.05.028

Russians News Agency. (2020). *Russian satellite maker develops lunar navigation system with at least 24 satellites*. https://tass.com

Schönfeldt, M., Grenier, A., Delépaut, A., Swinden, R., Giordano, P., & Ventura-Traveset, J. (2020a). Across the lunar landscape: Exploration with GNSS technology. *InsideGNSS*. https://insidegnss.com/across-the-lunar-landscape-exploration-with-gnss-technology

Schönfeldt, M., Grenier, A., Delépaut, A., Swinden, R., Giordano, P., & Ventura-Traveset, J. (2020b). Across the lunar landscape: Towards a dedicated Lunar PNT system. *InsideGNSS*. https://insidegnss.com/across-the-lunar-landscape-towards-a-dedicated-lunar-pnt-system

Space Frequency Coordination Group (SFCG). (2019). *Communication frequency allocations and sharing in the lunar region.* Space Frequency Coordination Group.

Spacewatch Europe. (2021). *Europe And Russia gear up for joint Luna-27 lunar lander*. https://spacewatch.global/2020/02/europe-and-russia-gear-up-for-joint-luna-27-lunar-lander

Vincent, F., Chaumette, E., & Vilà-Valls, J. (2019). Doppler-aided position estimation for HS-GNSS. *53rd Asilomar Conference on Signals, Systems, and Computers*, Pacific Grove, CA. https://doi.org/10.1109/IEEECONF44664.2019.9049044

Vincent, F., Vilà-Valls, J., Besson, O., Medina, D., & Chaumette, E. (2020). Doppler-aided positioning in GNSS receivers - A performance analysis. *Signal Processing, 176*. https://doi.org/10.1016/j.sigpro.2020.107713

Winternitz, L. B., Bamford, W. A., Long, A. C., & Hassouneh, M. (2019). GPS based autonomous navigation study for the lunar gateway. *Annual American Astronautical Society (AAS) Guidance, Navigation, and Control Conference.* Breckenridge, CO. https://ntrs.nasa.gov/citations/20190002311

How to cite this article: Grenier, A., Giordano, P., Bucci, L., Cropp, A., Zoccarato, P., Swinden, R., & Ventura-Traveset, J. (2022) Positioning and velocity performance levels for a lunar lander using a dedicated lunar communication and navigation system. *NAVIGATION, 69*(2). https://doi.org/10.33012/navi.513